

Continuous sPatial-Temporal Deformable Image Registration (CPT-DIR) for motion modelling in radiotherapy: beyond classic voxel-based methods

Xia Li^{1,2}, Muheng Li^{1,3}, Antony Lomax^{1,3}, Joachim Buhmann², Ye Zhang¹

1. Center for Proton Therapy, Paul Scherrer Institut
2. Department of Computer Science, ETH Zurich
3. Department of Physics, ETH Zurich

Short title: Continuous motion modeling using automatic deformable image registration.

Author to whom correspondence should be addressed. Email: ye.zhang@psi.ch

Keyword: Deformable Image Registration, Intra-fractional Motion Modeling, Implicit Neural Representation, Sliding Boundary, Large Deformation Diffeomorphic Metric Mapping

Word counts: 250 (abstract) / xxx (manuscript)

Acknowledgement:

This project is supported by the interdisciplinary doctoral grants (iDoc 2021-360) from the Personalized Health and Related Technologies (PHRT) of the ETH domain.

Highlights:

- Spatial continuous modeling solves the sliding boundary issue
- Temporal continuity releases the large deformation challenge
- Robust initialization and training easily usage
- High performance with fast optimization speed

Abstract

Background and purpose: Deformable image registration (DIR) is a crucial tool in radiotherapy for extracting and modelling organ motion. However, when significant changes and sliding boundaries are present, it faces compromised accuracy and uncertainty, determining the subsequential contour propagation and dose accumulation procedures.

Materials and methods: We propose an implicit neural representation (INR)-based approach modelling motion continuously in both space and time, named Continues-sPatial-Temporal DIR (CPT-DIR). This method uses a multilayer perception (MLP) network to map 3D coordinate (x, y, z) to its corresponding velocity vector (vx, vy, vz) . The displacement vectors $(\Delta x, \Delta y, \Delta z)$ are then calculated by integrating velocity vectors over time. The MLP's parameters can rapidly adapt to new cases without pre-training, enhancing optimisation. The DIR's performance was tested on the DIR-Lab dataset of 10 lung 4DCT cases, using metrics of landmark accuracy (TRE), contour conformity (Dice) and image similarity (MAE).

Results: The proposed CPT-DIR can reduce landmark TRE from 2.79 ± 1.88 mm to 0.99 ± 1.07 mm, outperforming B-splines' results for all cases. The MAE of the whole-body region improves from 35.46 ± 46.99 HU to 28.99 ± 32.70 HU. Furthermore, CPT-DIR surpasses B-splines for accuracy in the sliding boundary region, lowering MAE and increasing Dice coefficients for the ribcage from 65.65 ± 68.45 HU and 90.41% to 42.04 ± 45.60 HU and 90.56%, versus 75.40 ± 86.70 HU and 89.30% without registration. Meanwhile, CPT-DIR offers significant speed advantages, completing in under 15 seconds compared to a few minutes with the conventional B-splines method.

Conclusion: Leveraging the continuous representations, the CPT-DIR method significantly enhances registration accuracy, automation and speed, outperforming traditional B-splines in landmark and contour precision, particularly in the challenging areas.

Introduction

Deformable image registration (DIR) is a dynamic and evolving technique crucial in radiotherapy (RT) [1,2]. Serving as the vital component for processes in radiotherapy, such as contour propagation [3,4] and dose accumulation [5,6], DIR hinges on precisely estimating the dense displacement vector field (DVF) between two sequential intra-fractional or inter-fractional images. DIR remains a complex problem despite its importance due to the absence of definitive ground truth [7] and the high degree of freedom [8] in dense DVF optimisation. Current approaches in DIR can be broadly categorised into conventional iterative optimisation methods [9–16] and DL-based data-driven approaches [17–19]. The evolution of the DIR algorithms has transitioned from early foundational techniques like optical flow [9,10] and elastic models [11,12] to more sophisticated approaches such as the Demons algorithm [13,14] and B-splines based methods [15,16]. While these initial methods laid the groundwork, they were limited in their ability to handle complex scenarios, such as large deformation [20,21] and discontinued movement (so-called sliding boundary problem in RT) [22]. Despite their acceptable performance and generalisation, the conventional iterative optimization-based methods are characterised by the need for case-specific optimisation, leading to significant computational demands [23]. This often results in longer processing times, limiting its direct clinical applications. The accuracy and robustness of these methods also heavily depend on the quality of initial alignment, optimal parameter settings and constraint definition [24], necessitating expert intervention by adjusting hyper-parameters for individual cases.

DL-based data-driven approaches have significantly influenced recent technical advancements in DIR [24]. For example, VoxelMorph [19] is one of the notable advancements that utilised an unsupervised learning model to establish a better tradeoff between accuracy and speed. SynthMorph [18] extends deep learning capabilities in DIR by addressing challenges in multi-modal image registration. Transmorph [17] utilises the transformer models to enhance the long-range spatial correspondence modelling. All those works collectively represent the forefront of DIR algorithm development, showcasing the efficacy of deep learning in enhancing accuracy, reducing computational time, and improving generalizability across diverse medical imaging modalities. While advanced, DL-based DIR methods have limitations due to the unsupervised training with extensive training datasets, a challenge in medical contexts where data may be scarce or private [25]. Additionally, these DL-DIR methods often struggle to generalise to new data or different imaging modalities, limiting their actual clinical applicability in RT.

Recently, the emergence of Implicit Neural Representation (INR) [26,27] has not only revolutionised 3D reconstruction [28,29] but has also introduced a compelling solution in DIR [30]. This paradigm skillfully combines the benefits of iterative optimisation with the computational efficiency of neural networks, which can avoid the heavily supervised pre-training and significantly automatise DIR applications. For instance, IDIR [31] pioneered this trend by innovatively employing INR to learn and accurately fit the DVF. Building upon IDIR’s framework, ccDIR [32] introduces a cycle consistency loss to enhance the achievement of diffeomorphism in DIR. However, these methods still face challenges in both automatism and accuracy, particularly in sensitivity to hyper-parameters [32] and a lack of explicit design to address large deformation.

Building upon the concept of INR, we introduce a novel approach to representing the deformable registration process by an MLP network. We conceptualised it as a continuous flow in both spatial and temporal dimensions.

Leveraging the power of spatial continuity, our method aims to effectively address challenges of sliding boundary problems, a common issue encountered in classic DIR methods like B-splines. Additionally, temporal continuous modelling effectively mitigates the inherent limitations of voxel-based discretisation while offering a robust solution to challenges posed by large deformations. With its unsupervised property and automatically refined initialisation, the new CPT-DIR can quickly adapt to new cases without requiring individual heavy hyperparameter tuning.

Materials and Methods

Spatial continuous modeling

Draw inspiration from the success of INR in 3D reconstruction, we adopted concepts from IDIR and refined it for improved stability. Essentially, our approach involves mapping 3D coordinates to corresponding displacement vector using a learnable neural network, which can be formulated as:

$$(dx, dy, dz) = f_{\theta}(x, y, z)$$

The mapping function, denoted as f_{θ} , is implemented as a positional encoding followed by a 5-layer multi-layer perceptron (MLP) network [27], with each layer comprising 256 hidden states. Here, (x, y, z) represents not only coordinates on the volume grid but also any continuous location within the image space. All the resulting estimated displacement vector (dx, dy, dz) formed the dense DVF φ , which was used to warp the moving image I_1 into the warped image and compare to the fixed image I_0 . During training, the optimization problem can be written as:

$$L = \underset{\varphi}{\operatorname{argmin}} \|I_0 - I_1 \circ \varphi\| + \|\det(\operatorname{Jac}(\varphi_i)) - 1\|$$

Where $\circ \varphi$ denotes the warping by φ with bilinear resampling. Jac indicates the Jacobian matrix and \det represents the determinant. The first term measures the similarity between the warped and the fixed image I_0 . The second term ensures the determinant of the Jacobian matrix for displacement vectors approaching 1, thereby regulating motion towards a minimal distortion.

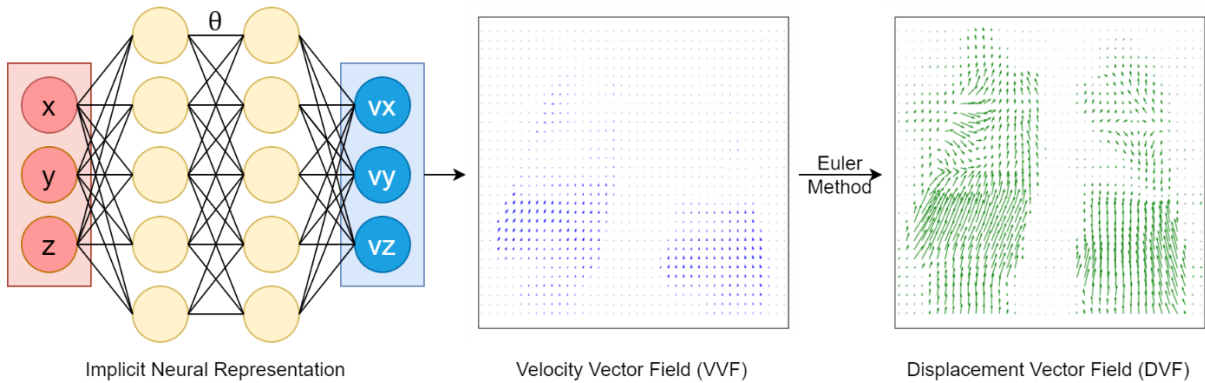


Figure 1. Overview of the proposed framework for spatial and temporal continuous motion modelling.

In contrast to classic DL-based methods that require training on large-scale datasets, our INR-based DIR only needs to fit one network per case. We implemented several strategies to stabilise the training process to address challenges encountered in the original IDIR, particularly its instability with large-deformation cases. Firstly,

instead of adopting a constant learning rate, we warmup it at 0 and linearly warm it up to 0.0001 over the first 500 steps. Subsequently, we employed a cosine scheduler [33] to decay the learning rate towards 0. Additionally, we adjusted the initialisation strategy by multiplying the voxel size to the weights of the final layer. This adjustment confines the initial output range to $[-\text{voxel size}, \text{voxel size}]$, ensuring the locality at the early stage for stability.

Temporal continuous modelling

The temporal continuous modelling employed in this study followed the principles of the Large Deformation Diffeomorphic Metric Mapping (LDDMM) [34,35], establishing a diffeomorphic mapping between the fixed and moving images. This mapping is achieved by estimating a time-dependent velocity vector field (VVF) and integrating it as the DVF, as shown in Figure 2. Mathematically, the integration process was facilitated by the Euler method, solving the ordinal differential equation, which can be expressed as:

$$\varphi = \int_0^1 v(t) dt$$

Here v is a space- and time-dependent velocity field. Figure 2 illustrates a visual example of an integrating process, where the network is operated as a ResNet [37]. Each step of the process predicts a residual related to the input coordinate. Consequently, the optimisation target is defined as:

$$L = \underset{v}{\operatorname{argmin}} \|I_0 - I_1 \circ \varphi\| + \frac{1}{2} \int_0^1 \|v(t)\|^2 dt$$

This objective function minimises the discrepancy between the fixed and warped images. Meanwhile, it also penalises the magnitude of the velocity field over the integration interval to avoid the contouring trajectory. An additional advantage of the spatial continuous modelling employed in our method is the ability to easily reverse the DVF using the reversed integration, defined as:

$$\varphi^{-1} = \int_1^0 -v(t) dt$$

This enables the derivation of the backward DVF (Figure 2) from a forward DVF, facilitating forward warping - a process that can be challenging with conventional modeling techniques.

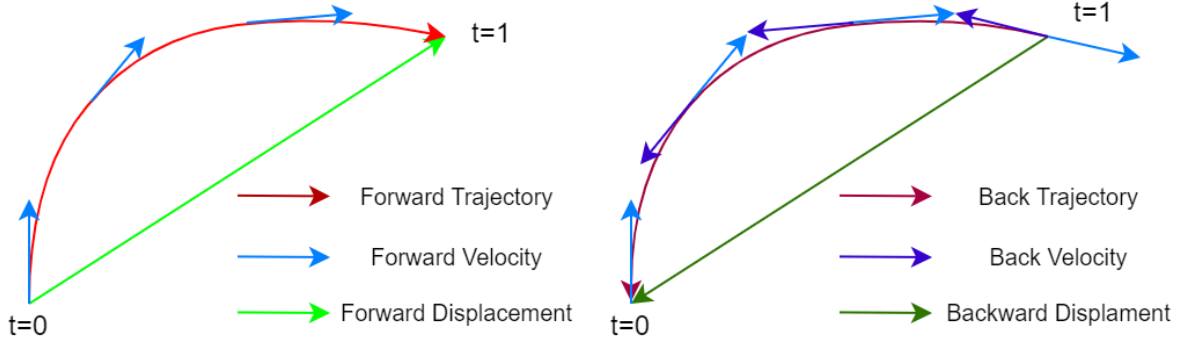


Figure 2. The mechanism of integrating velocity into displacement and the way of reversing it.

Image dataset

This study utilises the openly available DIR-Lab dataset [36], tailored for research in DIR algorithm development. The dataset comprises 4DCT scans from 10 patients undergoing treatment for esophageal malignancies. Each patient dataset consists of 10 respiratory phases, spanning from 0% to 90% of the respiratory cycle in increments of 10%. The resolution of the 4DCT is $1.0 \times 1.0 \times 2.5 \text{mm}$. The CT images have been pre-processed to include 300 manually identified landmark points for the two extreme phases (0% and 50%), facilitating the evaluation of the landmark accuracy. Following the dataset's convention, the 0% phase (end of inhalation) CT is selected as the

fixed image, while the 50% phase (end of exhalation) is chosen as the moving image. In addition to landmark points, a series of organs at risk (OARs) were extracted using Totalsegmentor [37] and reviewed and revised by physicians to ensure adherence to clinical standards.

Evaluation and statistics

The CPT-DIR algorithm was implemented into two specific models for validation and comparison: (a) the spatial continuous-only method as end-to-end (denoted as E2E); (b) the combined temporal and spatial continuous method as large deformation decomposition (denoted as LDD). Both models underwent two evaluation scenarios. In the first scenario, we followed the exact guidelines of the DIR-lab dataset to provide a fair comparison to previously submitted algorithms. The training was confined to the lung region only. Evaluation metrics in this scenario included Target Registration Error (TRE) for landmark accuracy and Mean Absolute Error (MAE) for image similarity in the lung region. In the second scenario, we evaluated the DIR registration performance for the RT dose accumulation application. The training was conducted on the entire body to assess the sliding boundary region (ribcage) performance fully. No auto- or manual segmentation was applied in this scenario. Evaluation criteria in this scenario included the landmark accuracy TRE and whole body MAE first. Then, the Dice coefficient and MAE were explicitly calculated for each OARs, including lung (left and right), esophagus, vertebra, hearts, spinal cord, and ribcage. We systematically compared the new CPT-DIR's performance against the performance of the classic B-Splines algorithm (implemented in Plastimatch [40]) and the corresponding metrics value for a scenario without registration.

Results

When training within the lung region alone, the landmark TRE for E2E and LDD models were recorded at $0.99\pm 1.11\text{mm}$ and $0.99\pm 1.07\text{mm}$, respectively, significantly reducing B-spline's TRE of $2.79\pm 1.88\text{mm}$ by more than half. By comparison, the original IDIR implementation [27] only achieved a TRE of $1.07\pm 1.11\text{mm}$. The leading state-of-the-art conventional method, iso PTV [41], achieved a TRE of 0.95mm within 3 minutes, whereas CPT-DIR can achieve similar performance within only 15 seconds on an RTX 4090 GPU. Regarding lung MAE, both E2E and LDD models reduced B-spline's results from $60.75\pm 59.06\text{HU}$ to $49.72\pm 39.56\text{HU}$ and $49.79\pm 39.73\text{HU}$, respectively. Detailed per-case results are shown in Figure 3.

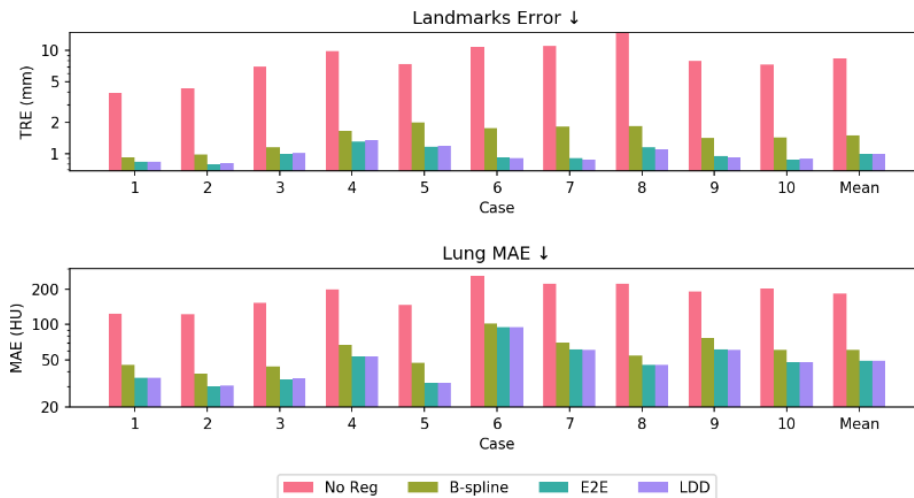


Figure 3. Quantitative comparisons of landmark accuracy and regional MAE between CPT-DIRs and classic B-

splines based DIR algorithm. For fairness, the training was conducted inside the lung region.

When training within the entire body, the whole-body MAE, both E2E (29.80±34.09HU) and LDD (28.99±32.70 HU) still considerably surpassed B-splines (35.46±46.99HU). The landmark accuracy degraded slightly for both the E2E and LDD models to 1.17±1.36mm and 1.17±1.45mm, respectively, yet remained lower than half of the B-spline’s performance. Detailed per-cased TRE, MAE, and per-OAR Dice, MAE are shown in Figure 4. Among all OARs, ribs are vital regions for assessing registration quality on sliding boundaries. Without registration, the MAE and Dice coefficients for ribs stood at 75.40HU and 89.30%, respectively. B-splines offered only marginal improvement, with metrics at 65.65HU and 90.41%. In contrast, E2E and LDD models dramatically reduced ribcages MAE to 43.62HU and 42.04HU, respectively, while increasing Dice coefficients to 90.34% and 90.56%. Notably, while most metrics show that LDD has a slight edge over E2E, the versatility of LDD is further emphasised by its landmark error of 1.17±1.15mm when executing a reverse trajectory.

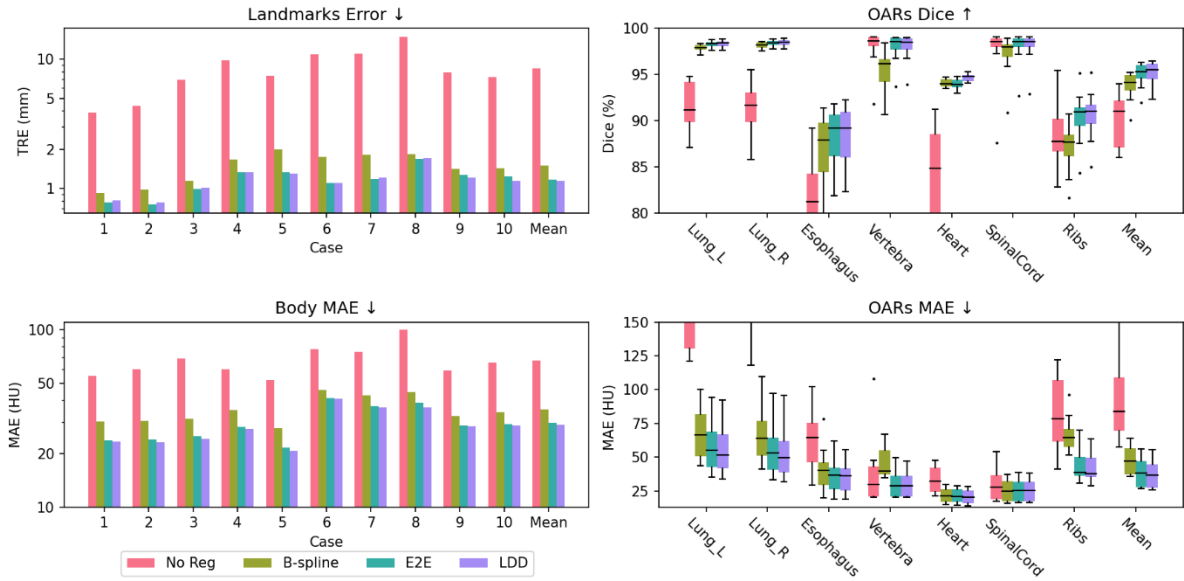


Figure 4. Quantitative comparison of landmark accuracy, regional MAE and OARs propagation accuracy between CPT-DIRs and classic B-splines based DIR algorithm. The training was conducted inside the whole-body region.

Regarding computational efficiency, B-splines took an average of 65.34±35.43s, while E2E and LDD processed at faster rates of 11.96±1.68s and 14.32±2.34s, respectively. Additionally, the visualisations of the resulted DVFs and error maps (between warped and fixed images) from different DIR methods can be found in [错误!未找到引用源。](#). The exemplified case-04 (the largest landmark TRE) and case-08 (the largest motion) show that the new CPT-DIR methods can significantly reduce the difference in the ribcage region.

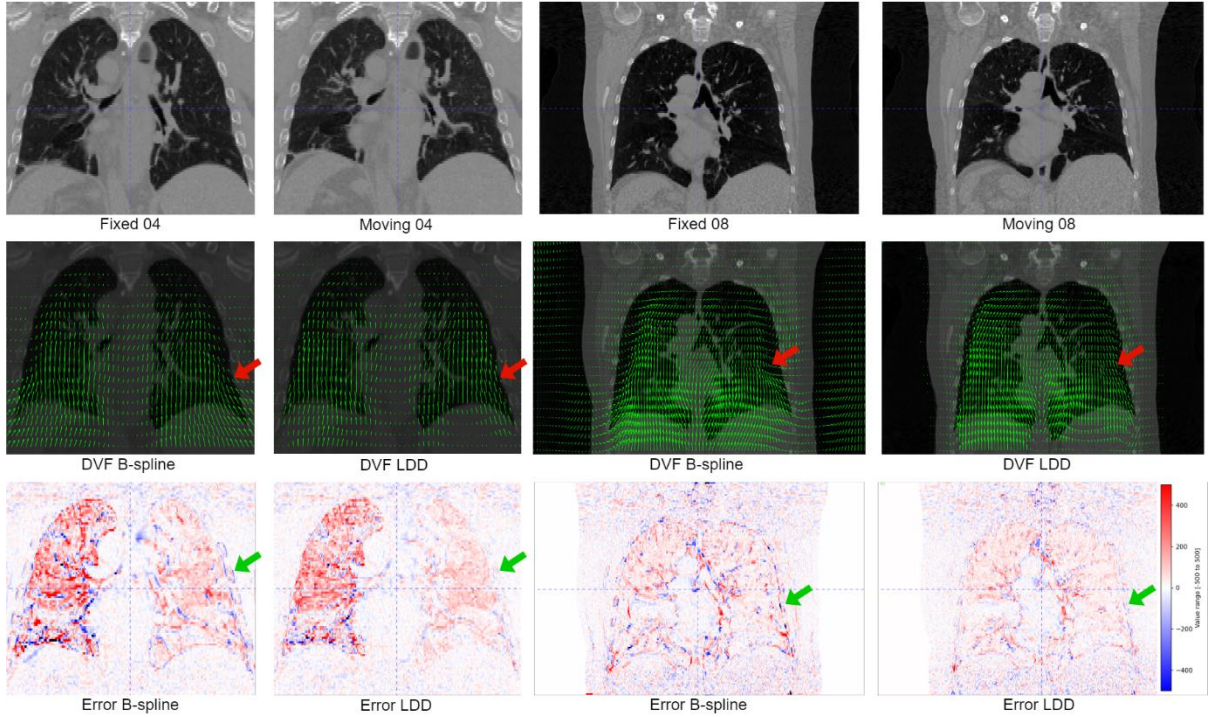


Figure 5. Visual comparison with B-splines over estimated DVFs and error maps. Arrows indicate the sliding boundary region.

Discussion

To enhance DIR performance for RT application, we draw inspiration from IDIR and LDDMM by incorporating spatial and temporal continuity into our LDD models. We aimed to improve intra-fraction motion modelling closer to the nature of physical anatomy. As elaborated in the introduction, the two prevailing learning paradigms for solving DIR problems are optimization-based and DL-based approaches. While optimization-based methods offer personalised modelling accuracy, they are time-consuming due to per-case parameter optimization. In contrast, DL-based methods leverage large datasets for training and provide real-time inference but may sacrifice performance. The newly proposed CPT-DIR method here is also optimised per case without individual setting parameter optimisation, aligning well with the former paradigm and offering personalized enhanced accuracy. This also satisfies the nature of radiotherapy, where a large dataset is challenging to collect, nor to clean and align the formats. Unlike previous optimization-based methods, our approach benefits from the computational efficiency of neural networks and GPU (benefits from DL-based methods), reducing processing time from minutes to seconds.

The DIR problem is inherently ill-posed and lacks a definitive ground truth, which necessitates the need for parameterisation of the searching space. The parameterisation serves as a form of implicit regularisation, effectively reducing the solution space. Voxel-based methods address this challenge by optimising each voxel independently, often necessitating additional regularisation terms to constrain voxel relationships. Namely, DL-based methods also operate in a voxel-based fashion. On the other hand, B-splines methods reduce the parametrisation space from individual voxels to splines, leading to overly smooth results and difficulty in

effectively handling sliding boundaries. In contrast, the new continuous motion modelling approach proposed here harnesses the power of neural networks to determine the smoothness/sharpness of each area automatically. Consequently, it can simultaneously model the smooth regions inside OARs and the sharp boundaries of the nearby organs.

Another significant challenge in DIR is the management of large deformations. Conventional methods like Demons rely on local assumptions, rendering them ineffective when faced with large deformations. This issue exacerbates the search space for matching locations in other DIR methods, and significant motion may disrupt local regularisation terms, affecting optimisation targets. LDDMM and Ordinal Differential Equation (ODE)-based methods address this challenge through decomposition, leveraging the typically more straightforward structure of the Velocity Vector Field (VVF) compared to the Displacement Vector Field (DVF). The effectiveness of modelling large deformations through temporal continuous modelling extends beyond motion estimation, encompassing other DIR tasks in radiotherapy, such as inter-fractional anatomic changes.

However, previous ODE-based methods [38,39] and LDDMM were limited by their reliance on voxel-based representations, rooted in the Euler specification from the theory of fluid mechanics. Despite being designed under the Lagrange specification to track each parcel separately, their implementation was confined to the Euler specification. Our spatial continuous modelling approach estimates the VVF at any point within the image and any time between two phases, not limited to grid points. Consequently, our implementation fully adheres to the Lagrange specification, enabling the tracking of each tissue component individually. We visualise the trajectory of landmarks in Supp A, demonstrating the potential of our approach for continuous motion tracking. This implementation opens avenues for further exploration in continuous motion tracking methodologies.

Another advantage of temporal continuous modelling is the ease of reversing the DVF [40]. Conventional methods typically require double effort to estimate bidirectional DVFs. However, in our framework, since the VVF can be directly reversed, reversing the DVF becomes straightforward. This capability enables tracking from any time between two phases and from any location inside the image to another time and location with just one-time training. This facilitates super-frame rate imaging (Supp A), potentially improving 4DCT reconstruction algorithms and 4D imaging pipelines in the future.

Quality assurance is crucial for commissioning DIR methods, especially for clinical applications. Landmarks provided by DIR-Lab serve as a reliable benchmark, but their accurate labelling requires substantial human efforts. Alternatively, organ masks can be generated using open-source segmentation tools like Totalsegmentor or other commercial tools, enabling rapid validation of fixed and moving images. In the absence of landmarks or organ masks, image similarity metrics can serve as a validation measure, albeit primarily effective in boundary regions. Moreover, robustness is another critical consideration when evaluating DIR performance. The original IDIR implementation [31] encountered higher failure rates in some cases in DIR-Lab, attributed to initialisation schemes. We addressed this issue by adjusting initial estimations within a two-voxel size range. Besides, the application of our proposed method in clinical pipelines requires the estimation of uncertainty, which represents the next step in our ongoing work.

Conclusion

In summary, the innovative CPT-DIR approach, integrating principles of INR and LDDMM, represents a

significant departure from traditional voxel-based methods in DIR. By adopting a paradigm of continuous motion modelling, we transcend the limitations inherent in voxel-based representations, offering a more robust, automatic and versatile solution. Leveraging spatial continuity, we effectively handle the intricacies of sliding organ boundaries, while temporal continuity alleviates the complexities associated with significant anatomical changes over time. The tangible benefits are evident in its superior performance compared to classic B-splines methods. CPT-DIR consistently achieves better performance by all kinds of evaluation matrices. Additionally, the efficiency gains are substantial, with registration times slashed by more than half. It can handle reverse trajectories, a capability previously unattainable with voxel-based approaches. This promises enhanced adaptability and robustness in image registration applications, particularly in radiotherapy applications. By eliminating the heavy need for manual tuning and leveraging unsupervised learning, we pave the way for further integration into automatic clinical workflows.

Reference

- [1] Rigaud B, Simon A, Castelli J, Lafond C, Acosta O, Haigron P, et al. Deformable image registration for radiation therapy: principle, methods, applications and evaluation. *Acta Oncol (Madr)* 2019;58:1225–37. <https://doi.org/10.1080/0284186X.2019.1620331>.
- [2] Oh S, Kim S. Deformable image registration in radiation therapy. *Radiat Oncol J* 2017;35:101. <https://doi.org/10.3857/ROJ.2017.00325>.
- [3] Kumarasiri A, Siddiqui F, Liu C, Yechieli R, Shah M, Pradhan D, et al. Deformable image registration based automatic CT-to-CT contour propagation for head and neck adaptive radiotherapy in the routine clinical setting. *Med Phys* 2014;41:121712. <https://doi.org/10.1118/1.4901409>.
- [4] Thor M, Petersen JBB, Bentzen L, Høyer M, Muren LP. Deformable image registration for contour propagation from CT to cone-beam CT scans in radiotherapy of prostate cancer. *Acta Oncol (Madr)* 2011;50:918–25. <https://doi.org/10.3109/0284186X.2011.577806>.
- [5] Bender ET, Hardcastle N, Tomé WA. On the dosimetric effect and reduction of inverse consistency and transitivity errors in deformable image registration for dose accumulation. *Med Phys* 2012;39:272–80. <https://doi.org/10.1118/1.3666948>.
- [6] Chetty IJ, Rosu-Bubulac M. Deformable Registration for Dose Accumulation. *Semin Radiat Oncol* 2019;29:198–208. <https://doi.org/10.1016/J.SEMRADONC.2019.02.002>.
- [7] Fischer B, Modersitzki J. Ill-posed medicine—an introduction to image registration. *Inverse Probl* 2008;24:034008. <https://doi.org/10.1088/0266-5611/24/3/034008>.
- [8] Sotiras A, Davatzikos C, Paragios N. Deformable medical image registration: A survey. *IEEE Trans Med Imaging* 2013;32:1153–90. <https://doi.org/10.1109/TMI.2013.2265603>.
- [9] Østergaard Noe K, De Senneville BD, Elstrøm UV, Tanderup K, Sørensen TS. Acceleration and validation of optical flow based deformable registration for image-guided radiotherapy. *Acta Oncol (Madr)* 2008;47:1286–93. <https://doi.org/10.1080/02841860802258760>.
- [10] Yang D, Li H, Low DA, Deasy JO, Naqa I EI. A fast inverse consistent deformable image registration method based on symmetric optical flow computation. *Phys Med Biol* 2008;53:6143. <https://doi.org/10.1088/0031-9155/53/21/017>.
- [11] Kybic J, Unser M. Fast parametric elastic image registration. *IEEE Transactions on Image Processing* 2003;12:1427–42. <https://doi.org/10.1109/TIP.2003.813139>.
- [12] Davatzikos C. Spatial Transformation and Registration of Brain Images Using Elastically Deformable Models. *Computer Vision and Image Understanding* 1997;66:207–22. <https://doi.org/10.1006/CVIU.1997.0605>.
- [13] Vercauteren T, Pennec X, Perchant A, Ayache N. Diffeomorphic demons: Efficient non-parametric image registration. *Neuroimage* 2009;45:S61–72.

- <https://doi.org/10.1016/J.NEUROIMAGE.2008.10.040>.
- [14] Vercauteren T, Pennec X, Perchant A, Ayache N. Non-parametric Diffeomorphic Image Registration with the Demons Algorithm. *Lecture Notes in Computer Science (Including Subseries Lecture Notes in Artificial Intelligence and Lecture Notes in Bioinformatics)* 2007;4792 LNCS:319–26. https://doi.org/10.1007/978-3-540-75759-7_39.
- [15] Rueckert D, Aljabar P, Heckemann RA, Hajnal J V., Hammers A. Diffeomorphic Registration Using B-Splines. *Lecture Notes in Computer Science (Including Subseries Lecture Notes in Artificial Intelligence and Lecture Notes in Bioinformatics)* 2006;4191 LNCS-II:702–9. https://doi.org/10.1007/11866763_86.
- [16] Klein S, Staring M, Pluim JPW. Evaluation of optimization methods for nonrigid medical image registration using mutual information and B-splines. *IEEE Transactions on Image Processing* 2007;16:2879–90. <https://doi.org/10.1109/TIP.2007.909412>.
- [17] Chen J, Frey EC, He Y, Segars WP, Li Y, Du Y. TransMorph: Transformer for unsupervised medical image registration. *Med Image Anal* 2022;82:102615. <https://doi.org/10.1016/J.MEDIA.2022.102615>.
- [18] Hoffmann M, Billot B, Greve DN, Iglesias JE, Fischl B, Dalca A V. SynthMorph: Learning contrast-invariant registration without acquired images. *IEEE Trans Med Imaging* 2022;41:543–58. <https://doi.org/10.1109/TMI.2021.3116879>.
- [19] Balakrishnan G, Zhao A, Sabuncu MR, Guttag J, Dalca A V. VoxelMorph: A Learning Framework for Deformable Medical Image Registration. *IEEE Trans Med Imaging* 2019;38:1788–800. <https://doi.org/10.1109/TMI.2019.2897538>.
- [20] Mok TCW, Chung ACS. Large Deformation Diffeomorphic Image Registration with Laplacian Pyramid Networks. *Lecture Notes in Computer Science (Including Subseries Lecture Notes in Artificial Intelligence and Lecture Notes in Bioinformatics)* 2020;12263 LNCS:211–21. https://doi.org/10.1007/978-3-030-59716-0_21/TABLES/1.
- [21] Zhong H, Weiss E, Siebers J V, Fu Y, Lei Y, Wang T, et al. Large deformation three-dimensional image registration in image-guided radiation therapy. *Phys Med Biol* 2005;50:5869. <https://doi.org/10.1088/0031-9155/50/24/008>.
- [22] McClelland JR, Blackall JM, Tarte S, Chandler AC, Hughes S, Ahmad S, et al. A continuous 4D motion model from multiple respiratory cycles for use in lung radiotherapy. *Med Phys* 2006;33:3348–58. <https://doi.org/10.1118/1.2222079>.
- [23] de Vos BD, Berendsen FF, Viergever MA, Sokooti H, Staring M, Išgum I. A deep learning framework for unsupervised affine and deformable image registration. *Med Image Anal* 2019;52:128–43. <https://doi.org/10.1016/J.MEDIA.2018.11.010>.
- [24] Fu Y, Lei Y, Wang T, Curran WJ, Liu T, Yang X. Deep learning in medical image registration: a review. *Phys Med Biol* 2020;65:20TR01.

- <https://doi.org/10.1088/1361-6560/AB843E>.
- [25] Zajac HD, Avlona NR, Andersen TO, Kensing F. Ground Truth Or Dare: Factors Affecting The Creation Of Medical Datasets For Training AI n.d. <https://doi.org/10.1145/3600211.3604766>.
- [26] Molaei A, Aminimehr A, Tavakoli A, Kazerouni A, Azad B, Azad R, et al. Implicit Neural Representation in Medical Imaging: A Comparative Survey 2023:2381–91.
- [27] Sitzmann V, Martel JNP, Bergman AW, Lindell DB, Wetzstein G. Implicit Neural Representations with Periodic Activation Functions. *Adv Neural Inf Process Syst* 2020;33:7462–73.
- [28] Yu A, Ye V, Tancik M, Kanazawa A. pixelNeRF: Neural Radiance Fields From One or Few Images 2021:4578–87.
- [29] Mildenhall B, Srinivasan PP, Tancik M, Barron JT, Ramamoorthi R, Ng R. NeRF. *Commun ACM* 2021;65:99–106. <https://doi.org/10.1145/3503250>.
- [30] Park K, Sinha U, Barron JT, Bouaziz S, Goldman DB, Seitz SM, et al. Nerfies: Deformable Neural Radiance Fields 2021:5865–74.
- [31] Wolterink JM, Zwienenberg JC, Brune C. Implicit Neural Representations for Deformable Image Registration. *Proc Mach Learn Res* 2022;172:1–11.
- [32] Van Harten LD, Stoker J, Išgum I. IEEE TRANSACTIONS ON MEDICAL IMAGING, (ACCEPTED-IN PRESS) Robust deformable image registration using cycle-consistent implicit representations n.d.
- [33] Loshchilov I, Hutter F. SGDR: Stochastic Gradient Descent with Warm Restarts. 5th International Conference on Learning Representations, ICLR 2017 - Conference Track Proceedings 2016.
- [34] Beg MF, Miller MI, Trouvé A, Younes L. Computing large deformation metric mappings via geodesic flows of diffeomorphisms. *Int J Comput Vis* 2005;61:139–57. <https://doi.org/10.1023/B:VISI.0000043755.93987.AA/METRICS>.
- [35] Dupuis P, Grenander U, Miller MI. VARIATIONAL PROBLEMS ON FLOWS OF DIFFEOMORPHISMS FOR IMAGE MATCHING. *Appl Math (Irvine)* 1998;56:587–600.
- [36] Castillo R, Castillo E, Guerra R, Johnson VE, McPhail T, Garg AK, et al. A framework for evaluation of deformable image registration spatial accuracy using large landmark point sets. *Phys Med Biol* 2009;54:1849. <https://doi.org/10.1088/0031-9155/54/7/001>.
- [37] Wasserthal J, Breit HC, Meyer MT, Pradella M, Hinck D, Sauter AW, et al. TotalSegmentator: Robust Segmentation of 104 Anatomic Structures in CT Images. *Radiol Artif Intell* 2023;5. <https://doi.org/10.1148/RYAI.230024>.
- [38] Wu Y, Jiahao TZ, Wang J, Yushkevich PA, Hsieh MA, Gee JC. NODEO: A Neural Ordinary Differential Equation Based Optimization Framework for Deformable Image Registration 2022:20804–13.
- [39] Liang X, Lin S, Liu F, Schreiber D, Yip M. ORRN: An ODE-Based Recursive Registration Network for Deformable Respiratory Motion Estimation with Lung 4DCT Images. *IEEE Trans Biomed Eng* 2023;70:3265–76.

<https://doi.org/10.1109/TBME.2023.3280463>.

- [40] Murr M, Brock KK, Fusella M, Hardcastle N, Hussein M, Jameson MG, et al. Applicability and usage of dose mapping/accumulation in radiotherapy. *Radiotherapy and Oncology* 2023;182:109527. <https://doi.org/10.1016/j.radonc.2023.109527>.

Supplementary Materials

A. Landmark trajectory visualisation with super frame rate

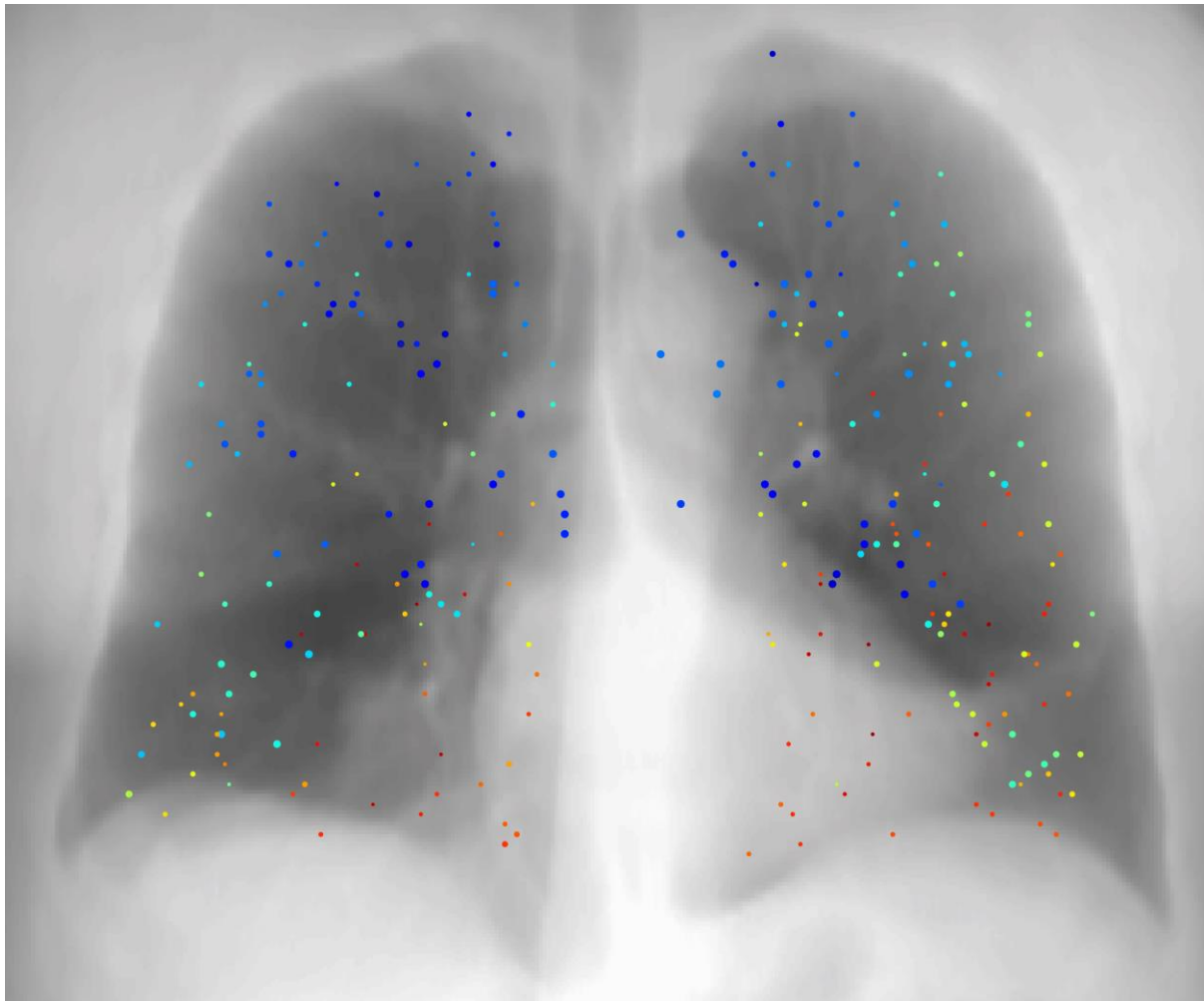


Figure A. Visualisation of landmarks' trajectory from the inhale phase (0%) to the exhale (50%) phase. The network only fits between the two extreme phase. 32 middle phases are interpolated with the benefit from our CPT-DIR's continuous modeling.